Journal Pre-proof

On preventing thermal damage in high-temperature joining applications of thermoplastic composites with metals

Dimitrios Gaitanelis, Chris Worrall, Mihalis Kazilas

PII: S1359-8368(25)00423-8

DOI: https://doi.org/10.1016/j.compositesb.2025.112522

Reference: JCOMB 112522

To appear in: *Composites Part B*

Received Date: 3 May 2024

Revised Date: 9 April 2025

Accepted Date: 12 April 2025

Please cite this article as: Gaitanelis D, Worrall C, Kazilas M, On preventing thermal damage in high-temperature joining applications of thermoplastic composites with metals, *Composites Part B*, https://doi.org/10.1016/j.compositesb.2025.112522.

On preventing thermal damage in high-temperature joining applications of thermoplastic composites with metals

Dimitrios Gaitanelis [a, b, *], Chris Worrall [c] and Mihalis Kazilas [d]

[a] Advanced Manufacturing Research Centre with Boeing, University of Sheffield, Catcliff, Rotherham S60 5TZ

[b] NSIRC, TWI Ltd, Granta Park, Great Abington, Cambridge, CB21 6AL

[c] Advanced Composites and Adhesives section, TWI Ltd, Cambridge, CB21 6AL

[d] Brunel Composites Centre, Brunel University London, London, UB8 3PH

* Corresponding author: Dimitrios Gaitanelis (d.gaitanelis@sheffield.ac.uk)

Abstract

This paper addresses the critical need for a comprehensive investigation into the thermal limits of thermoplastic composites in thermal joining applications with metals. A numerical framework is employed to identify processing conditions that prevent thermal degradation in composite-metal joining, demonstrated through a case study of laser joining carbon fibre (CF) reinforced poly-ether-ether-ketone (PEEK) with a Ti6AL4V Titanium (Ti) alloy. The PEEK kinetics are integrated in the numerical solver and a coupled thermal-chemical analysis takes place that accounts for the heating rate effect on the material's thermal response. To validate the model, an experimental investigation takes place where the two materials are joined with a varying laser power. To assess the extent of thermal degradation, the produced joints are examined with optical microscopy, scanning electron microscopy, and attenuated total reflection – Fourier transform infrared spectroscopy. To correlate the resulting thermal degradation with their mechanical response, lap-shear tests are performed. A good agreement is found between the two investigations: the model accurately identifies 500 W as the critical threshold where thermal degradation initiates ($\alpha \approx 1.2\%$), leading to a 9% drop in joint strength. Optimal joint performance is achieved at 450 W - just below the degradation threshold - while higher powers result in severe thermal damage and porosities, causing performance losses of up to 76%. These findings demonstrate that the proposed methodology can effectively determine the thermal limits of CF/PEEK in fast heating applications where the exact temperature-time combination that would lead to thermal damage is elusive. Therefore, the model could be used to optimise a range of joining applications

where high-temperature - short-duration processing is applied and thermal degradation is a potential issue.

Keywords

Thermal degradation; A. Polymer-matrix composites (PMCs); A. Thermoplastic resin; E. Joints/joining; E. Heat treatment.

1. Introduction

With the aim of advancing sustainability, automotive and aerospace industries are increasingly looking to use carbon fibre (CF) composites to achieve up to 50% weight savings over metallic alternatives. Nonetheless, it is unlikely that these industries will adopt a 100% composite solution and the optimum design will inevitably comprise both composites and metals. Currently, mechanical fastening and adhesive bonding are the predominant methods for joining composites to metals. Yet, they suffer from several drawbacks. Mechanical fastening introduces bolts and rivets to the structure that increase the weight [1], and can act as crack initiation points [2]. This can be addressed with adhesive bonding, that does not induce a flaw in the structure. However, it requires surface treatments at optimal conditions [1] making the process cost-ineffective [3]. Hence, there is a clear need for new, flexible, cost-effective, and rapid methods for joining composites to metals which often involve high temperatures.

Some of these methods include induction welding [4], friction spot welding [5–9], resistance welding [10–15], and ultrasonic metal welding [16,17]. Also, laser joining as a flexible non-contact process where localised heating is applied, has received a considerable attention from industry and academia [18–22]. A fundamental problem with these approaches is that, either during the joining process itself or in subsequent joining processes, the metal part is exposed to temperatures higher than the adjoining polymer composite can normally tolerate. This can trigger the thermal degradation mechanisms of the polymer matrix which is an important damage mechanism in these applications [18,23–26]. It could result in porosities that could cause delamination and therefore deteriorate the joint performance [18,27,28]. Altogether, the process window for achieving a high-quality joint in composite-metal thermal joining is narrow. On the one hand, it is constrained by the parameters that would bond the materials and on the other hand by those that would trigger the polymer's degradation mechanisms.

Therefore, to identify the optimum process window a thorough investigation is required which usually

takes place experimentally [10,13,18,19,28–35]. A crucial aspect in this experimental optimisation is capturing the temperature distribution in the joint's interface region, yet it poses significant challenges [36]. In conventional setups, pyrometers and infrared cameras cannot easily target on the interface of the joint and placing thermocouples in that area inevitably influences the materials' contact therefore affecting the resulting temperature distribution [37]. Given this challenge, along with the increased cost and complexity of experimental investigations, Finite Element Analysis (FEA) could be a useful alternative for identifying the thermal limits of composites in their thermal joining applications with metals. Additionally, developing a universal numerical methodology - one that could be applied across various material joining systems and joining methods – would be a significant contribution to the field. Such a methodology would serve to identify the processing conditions capable of reaching elevated temperatures without inducing substantial thermal damage to the composite part of the joint [38].

So far, studies that have examined numerically high-temperature joining applications of composites with metals have mostly used FEA to derive the composite material's temperature field during joining [37,39–46]. Typically, these models incorporate the polymer's melting point (T_m) and the temperature where the onset of thermal degradation occurs as the material's thermal limits [32,47,48]. These critical temperatures are usually obtained with thermogravimetric analysis (TGA) or differential scanning calorimetry (DSC), where the applied heating rates are commonly below 50°C/min [49–52]. Nevertheless, in joining applications such as laser joining or induction welding, the heating rates can exceed 1000°C/min, and the joining composite may reach its maximum temperatures in less than a second [24]. Therefore, exceeding the polymer's T_m for a very short amount of time may not ensure the necessary melting and softening for a successful composite-metal joint. Likewise, given the increased heating rates, a short dwell time at temperatures higher than those found critical by TGA or DSC might not necessarily trigger the polymer's thermal degradation. Hence, to determine the thermal limits of composites in thermal joining applications with metals it is important to account for both the attained temperatures and dwell time. Consequently, when examining numerically these applications, it is vital to consider the effect of the heating rate on the material's degradation mechanisms [23,26,38].

To do so, this work uses a numerical framework recently developed by the authors [38] to detect the parameters that prevent thermal damage in composite-metal joining. Its applicability is demonstrated in laser joining of CF-reinforced poly-ether-ether-ketone (PEEK) with a Ti6AL4V Titanium (Ti) alloy.

Section 2 offers a brief overview of the theoretical background. Section 3 describes the materials and methods used, and section 4 and 5 present the numerical and experimental results. A comparison between the two investigations is found in section 6 and the main conclusions are gathered in section 7.

2. Theoretical background

When polymer matrix composites (PMCs) experience fast heating conditions where increased heating rates occur, the onset of thermal degradation - as manifested by mass loss - offsets to elevated temperatures [23,26,38]. To address this numerically, the authors have developed a methodology that calculates the decomposition degree α and uses it as a field variable for updating the material properties of the examined CF-reinforced polymer (CFRP) in each time increment [38]. The decomposition degree α is defined with

$$\alpha = \left[\frac{\rho_{virgin}-\rho}{\rho_{virgin}-\rho_{charred}}\right] \quad [1]$$

where ρ is the instant density and ρ_{virgin} and $\rho_{charred}$ is the density of the virgin and the charred (fully decomposed) material state respectively. To calculate the values of α in each increment, the kinetic model $K(T)$ defined by the Arrhenius-type equation

$$K(T) = A\,exp\left(\frac{-E_a}{RT}\right) \quad [2]$$

is employed. Its relationship with the decomposition degree α is established with the equation

$$\frac{d\alpha}{dt} = K(T)(1-\alpha)^n \quad [3]$$

where the rate of α over time is represented as the n-th power of the non-decomposed material $(1-\alpha)$ [38,53]. In *Eq. 2* and *Eq. 3*, R is the universal gas constant while A, E_a, and n are the kinetic parameters of the examined material (activation energy, pre-exponential factor, and reaction order respectively). These parameters are derived from TGA at conventional heating rates, and their implementation in the numerical solver takes place by solving the integrated form of *Eq. 3* (t = 0, α = 0), shown in

$$\alpha = 1-\left[(n-1)Aexp\left(\frac{-E_a}{RT}\right)t+1\right]^{\frac{1}{1-n}} \quad [4]$$

To solve this equation in each time increment Δt and calculate the current value of the decomposition degree α, the solver uses the temperature values of the current (T_i) and previous increment (T_{i-1}) and the decomposition degree of the previous step (α_{i-1}) [38]. In essence, this methodology integrates the material's kinetics into the model, capturing the evolution of the decomposition degree field throughout

the simulation [38]. Through this process, a coupled thermal-chemical analysis takes place which employs an extrapolation approach to examine the response of PMCs at extreme heating rates.

3. Materials and methods

The Ti6Al4V sheets used are provided by Smiths metals Ltd., UK, and the CF/PEEK laminate is supplied by Ensinger Plastics Ltd., Switzerland. An APC-2/IM7 laminate with 16 layers is used with a 50% fibre volume fraction (V_f), and a uniform stacking sequence of $[0°/90°]_{4s}$. The ply thickness is 0.136 mm and the CF/PEEK laminate was press moulded at 380°C and 20 bar. Prior to joining, the Ti alloy is blasted with alumina oxide particles with a grit of 100 μm and is ultrasonically cleaned for two hours. Finally, to reduce their moisture content, the CF/PEEK plates are dried at 65 °C for two hours.

The laser joining takes place between Ti sheets of 75 mm × 25 mm × 1.6 mm and CF/PEEK plates of 75 mm × 25 mm × 2.2 mm. The process is modelled in Abaqus, and the numerically examined case study is experimentally reproduced using an IPG YLS-2000 continuous wave (CW) fiber laser. The joints' performance is examined with lap-shear tests, while optical microscopy (OM) and scanning electron microscopy (SEM) are employed to examine the fractured surfaces, the interfacial microstructure, and the damage mechanisms that occur. To assess the extent of thermal degradation, the joined CF/PEEK plates are examined with attenuated total reflection-Fourier transform infrared spectroscopy (ATR-FTIR). Through this process, the joints' mechanical response is correlated with the extent of thermal degradation occurring in CF/PEEK, highlighting its impact on the joint performance.

4. Numerical investigation

4.1. Developed model

A transient heat transfer analysis of the laser joining process is carried out in Abaqus® for 10 seconds. As in the experiments, a 16 mm lap width is considered in the model and a schematic of the examined case study is shown in Fig. 1a. To model the laser heat flux, Q_{Laser}, subroutine DFLUX is used, and a circular two-dimensional (2D) Gaussian beam is applied on the Ti alloy at the x-z plane with

$$Q_{Laser} = \frac{2n_{Laser}\, P_{Laser}}{\pi r_{Laser}^2} exp\left[-2\left(\frac{(x-x_0)^2+(z-z_0)^2}{r_{Laser}^2}\right)\right] \quad [5]$$

where, P_{Laser} and r_{Laser} are the laser power and the laser beam radius respectively and n_{Laser} is the laser absorptivity of the Ti6Al4V alloy which equals 0.5 [54,55]. As in the experimental investigation, the applied beam diameter equals 8 mm, and the laser beam is modelled to travel across the central line

of the joint's overlapping region with a scanning speed of 10 mm/s. To identify the optimum laser joining parameters, a laser power of 400 W, 450 W, 500 W, 600 W, 700 W, and 800 W is examined.

4.1.1. Mesh characteristics and boundary conditions

Solid elements, and particularly 8-node linear heat transfer brick elements (DC3D8) are applied in the model. To achieve computational efficiency without compromising accuracy, a mesh sensitivity analysis was conducted in the overlapping region using an element size ranging from 0.1 mm to 0.5 mm. Variations in peak temperatures remained minimal between the 0.1 mm and 0.3 mm meshes, indicating numerical convergence. Therefore, a 0.3 mm element size was selected in the overlapping region (Fig. 1*b*) as it offered a good compromise between accuracy and computational cost. In the rest of the model, an element size of 1.5 mm is applied. The Ti alloy is partitioned in ten regions of equal thickness, while the top eight plies of the CF/PEEK plate are modelled with two elements in their through-thickness direction (element thickness: 0.068 mm). These top eight plies follow the fibre orientation of the examined CF/PEEK plate. The remaining plies of CF/PEEK are partitioned in four regions of 0.27 mm thickness with a $[90°/0°]_2$ layup (Fig. 1*b*). To represent the experimental conditions, surface radiation and air convection are applied to the top and the lateral surfaces of the materials while the bottom surfaces are modelled as adiabatic. An air convection coefficient equal to 50 $W/m^2{\cdot}K$ is used, while an emissivity equal to 0.95 is considered for CF/PEEK. When P_{Laser} > 500 W and the surface temperature of Titanium surpasses 1000 °C, an emissivity of 0.98 is applied in the laser-heated region of Ti [56]. On the other hand, an emissivity equal to 0.62 is considered when $P_{Laser} \leq 500$ W. The rest of the Ti alloy is modelled with an emissivity of 0.25 [56].

4.1.2. Material properties, applied extrapolation approach, and numerical framework

The Ti6Al4V alloy is modelled with temperature-dependent material properties, derived from the study of Yang et al. [56]. Additionally, a perfect interface is assumed in this study given that altering the thermal contact conductance (TCC) did not significantly affect the temperature field in CF/PEEK. Regarding CF/PEEK, this study uses the numerical framework of [38] to model its thermal response, which employs decomposition-dependent material properties (Table 1). As discussed in section 2, the kinetic model of PEEK – calculated with TGA at conventional heating rates – is implemented in Abaqus and an extrapolation approach is applied to examine the response of CF/PEEK in the examined

conditions. This takes place with the user-defined subroutines USDFLD and HETVAL and a detailed description can be found in [38]. This approach is advantageous as it accounts for the material's response to the heating rate. Particularly in joining applications where a short-time exposure to elevated temperatures occurs, this method serves for capturing thermal limits, therefore enabling a better control over the joining process. Especially in composite-metal laser joining, this is essential for detecting the optimum processing parameters given the challenge of experimentally measuring the resulting temperature field in the interface of the joint - the most thermally impacted region for the composite.

4.2. *Numerical model results*

The main outputs of the numerical investigation are gathered in Table 2. Regarding the Ti alloy, oxidation occurs at 760°C and the emissivity of Titanium increases rapidly [56]. At temperatures ≥ 980°C defects are found that correspond to the material's heat-affected zone (HAZ) [56]. The results show that 980°C are surpassed at a laser power > 500 W (Table 2). Interestingly, HAZ is found on the Ti surface at these powers which serves as a preliminary validation of the developed model (Fig. 5). Nevertheless, this study's objective is to detect the parameters that surpass PEEK's thermal degradation threshold where $\alpha \geq 0{,}01$. First, Fig. 2 presents the temperature profiles across the top region of the CF/PEEK laminate - corresponding to 31% of the plate's total thickness – following the laser heating of the Ti alloy. These curves provide both the peak temperatures and the corresponding dwell times in the examined region. To date, a few studies have examined the maximum process time of CF/PEEK when it is heated at temperatures higher than 400°C [57,58], while most studies have focused on cases where long-time heating takes place at lower temperatures [50,59–61]. Since exposing the material at elevated temperatures for short durations might not necessarily trigger its degradation mechanisms, the focus is given on the resulting decomposition degree field on the region of the CF/PEEK laminate closest to the joint's interface, which represents the most severely impacted area for a composite material during laser joining with metals.

The resulting degradation profile at the examined laser powers is shown in Fig. 3. The decomposition degree α varies between zero and one, with zero corresponding to the virgin material and one to the fully decomposed [38]. From a previous authors' study, it was found that a 1% decomposition does not induce a significant thermal damage on PEEK, especially when rapid heating is applied [23,26,38]. Likewise, previous works have also considered a decomposition degree α of 0.01 as the threshold for

ensuring the post-processing structural integrity of CF/PEEK [58,62,63]. Consequently, a value of α equal to 0.01 is considered as the thermal limit in this work. This is slightly surpassed (α = 0.012) at 500 W (Fig. 3c). Hence, according to the numerical model, laser powers slightly less than 500 W can achieve temperatures high enough for the joining to take place without triggering the thermal degradation mechanisms of PEEK. Opposite to that, a higher applied thermal load with a further increase in power results in a severe thermal damage, reaching 58.7% at 600 W (Fig. 3d), 97.2% at 700 W (Fig. 3d), and 99.8% at 800 W (Fig. 3f) compromising joint performance. To validate these results, an experimental investigation takes place.

5. Experimental investigation

5.1. Laser joining experiment

The experimental setup of the laser joining process is depicted in Fig. 4. An IPG YLS-2000 CW fiber laser is used with a maximum power of 2000 W and a wavelength of 1070 nm. The distance between the laser head and the specimen is 470 mm and the defocus distance is 20 mm, resulting in a laser spot diameter equal to 8 mm on the Ti surface. To prevent the oxidation of Titanium, Argon shielding gas is supplied during the joining process (Fig. 4a). Clamping jigs are used to ensure a good contact between the materials and to achieve the same pressure across the joint's overlapping region, each bolt is tightened with 4 N•m using a torque wrench (Fig. 4b). The overlapping region of the joint is equal to 16 mm and the dimensions of the two plates are shown in Fig. 1b. Before the laser joining, the Ti sheets are degreased with acetone and the surface of the CF/PEEK plates is cleaned with Isopropyl Achohol. As in the numerical investigation, a scanning speed of 10 mm/s is applied together with a laser power of 400 W, 450 W, 500 W, 600 W, 700 W, and 800 W.

5.2. Results and discussion

5.2.1. Effect of the applied laser heating on the surface of the Ti6Al4V Ti alloy

Fig. 5 shows the Ti surface of the produced joints. HAZ occurs for laser powers ≥ 600 W, while oxidation is only found at laser powers < 600 W. The characteristic yellow colour in the melt pool of the Ti alloy is evident at 450 W and 500 W (Fig. 5b, Fig. 5c) as well as at 400 W to a lesser extent (Fig. 5a). Interestingly, the model captures the temperatures that would lead to defects when $P_{Laser} \geq 600$ W (Table 2). It also accurately predicts the slight oxidation at 400 W, and the more significant oxidation at

450 W and 500 W, where temperatures surpassed 780°C (Table 2). This provides an initial validation of the applied numerical recipe which, regarding the Ti alloy, is based on the study of Yang et al [56].

5.2.2. *Cross-sectional analysis of the produced joints*

The cross-sections of the joints - vertical and in the middle of the laser pathway - are examined in Fig. 6. Overall, increasing the applied laser power increases the thermally affected region in the composite part of the joint. At 400 W, only melting is observed at the top CF/PEEK ply, with no thermal defects detected through the thickness (Fig. 6a). With the power rising to 450 W and 500 W, the HAZ expands but remains constrained to the first ply of CF/PEEK (Fig. 6b, Fig. 6c). Nevertheless, as indicated in the details of Fig. 6c, porosities develop in the 500 W specimen. These porosities result from PEEK's thermal degradation and can significantly affect the performance of the joints [18]. In a greater extent, they are also identified in the 600 W specimen whose thermally affected region reaches the second ply of the composite laminate (Fig. 6d). Further increasing the laser power leads to more severe thermal damage with the HAZ reaching the fifth ply in the 700 W and 800 W joints (Fig. 6e, Fig. 6f).

A detailed SEM imaging of the joints' cross-sections is presented in Fig. 7. The melting that occurs at the interface of the 400 W joint is depicted in Fig. 7a, while the top ply's HAZ found at the 450 W and 500 W joints is shown in Fig. 7b and Fig. 7c. The thermally impacted plies at 600 W are shown in Fig. 7d, while thermal degradation porosities are observed at laser powers > 500 W (Fig. 7c- Fig. 7f). Finally, the 700 W and 800 W joints display exposed fibres and fully degraded PEEK matrix, along with an extensive non-bonded region that hinders the interface bond (Fig. 7e, Fig. 7f). The latter is attributed to the deeply penetrating laser heating on the Ti alloy which has reached the joint interface. This is acting as a form of impact during the joining process, therefore resulting in insufficient contact between the materials (Fig. 7e). This phenomenon is expected to compromise the post-processing structural integrity of these joints, as later confirmed by lap-shear tests.

5.2.3. *Formed porosities and observed porosities formation mechanisms*

Thermal degradation porosities and shrinkage porosities are the two main types of porosities found in the examined case study (Fig. 8). In Fig. 8a and Fig. 8b, porosities resulting from thermal degradation are observed in the 500 W and 600 W joints. Their formation occurs due to the diffusion of decomposition gases that takes place upon PEEK's thermal degradation [38]. Similarly to the study of Tan et al. [18], these porosities have a characteristic peanut shape and a length of approximately 100

μm. They are mainly found between the adjacent plies of CF/PEEK (Fig. 7, Fig. 8b) and in the interface region of the materials (Fig. 7), with the latter having the potential to act as delamination initiation and propagation points thus deteriorating the load-bearing capability of the joints [18,38,64].

Shrinkage porosities resulting from the solidification sequence that the composite material experiences during the joining process are also found in this work. During cooling, the composite plate closer to the Ti alloy solidifies first, and the established solidification sequence results in shrinkage porosities within the inner boundaries of CF/PEEK's thermally affected region or near the joint's interface [18]. Fig. 8d shows an example of such a porosity within the second ply of the 500 W joint, depicted also in Fig. 7c. This porosity exhibits a rough surface with cracks and an irregular shape compared to thermal degradation porosities (Fig. 8a), which is characteristic of this type of porosities [18].

Another type of shrinkage porosities is also identified, attributed to the formation of thermal residual stresses. These stresses occur due to the existing mismatch in the coefficients of thermal expansion (CTE) of CF and PEEK [65]. They lead to the volume shrinkage of the PEEK matrix which causes the smaller-size shrinkage porosities that are found in this work. This mechanism has been recently depicted in the micro level in CF/PEEK [66] and its presence in the meso level is evident in Fig. 8c and Fig. 8e. For example, in the resin pockets of the 800 W joint, where closely packed fibres exist, thermal residual stresses occur in various directions around the pocket's periphery resulting in small-size shrinkage porosities (Fig. 8e). Likewise, in Fig. 8c wrinkled surfaces indicative of thermal residual stresses are evident in the top part of the porosity near an area with increased fibre content, while they are absent from the bottom part and edges - areas without proximity to CFs (Fig. 8a).

5.2.4. *Mechanical performance: Lap-shear tests*

The lap-shear tests take place using an Instron 8801 servo hydraulic test frame with a load capacity between 0.2 kN and 100 kN, and a gripping length of 30 mm used in each side (Fig. 9a). Three joints are examined for each power with a loading rate of 1.3 mm/min. Representative tensile shear load - displacement curves are presented in Fig. 9b, while the average value and the standard deviation reached in each group is shown in Fig. 9c. The optimum joint performance is achieved at 450 W, with an average tensile shear load of 2030 N, 32.1% higher than at 400 W (1378 N). Joints produced at 500 W show the second-best performance, with an average load of 1849 N. Further increase in laser power

impacts the joints, with loads dropping to 1264 N at 600 W, 646 N at 700 W, and 490 N at 800 W.

This trend reflects the typical behavior in composite-metal laser joining, where lower powers or higher scanning speeds may lead to weak bonding if they melt an insufficient region of the composite. Higher powers or slower scanning speeds widen the joining area improving the joint's strength but risk triggering the thermal degradation of the polymer matrix, causing porosities and other damage mechanisms that impact the joints. Indeed, the 400 W joints exhibit moderate performance, indicating insufficient power for a strong bond. Increasing the power to 450 W yields optimal performance, while further increase to 500 W leads to a 9% performance decrease due to the triggered thermal degradation mechanisms in the PEEK matrix. Even higher laser powers induce severe thermal damage, deteriorating further the load-bearing capability of the joints. Interestingly, 500 W is captured as the critical laser power by both the numerical analysis and SEM. For example, the model captures the onset of thermal degradation at 500 W (Fig. 3c), and thermal degradation porosities first form in the through-thickens direction of CF/PEEK at 500 W (Fig. 6c). This validates the model and highlights its significance.

5.2.5. *Fractured surfaces of the produced joints*

Fig. 10 shows the fractured surfaces of the joints after the lap-shear tests, providing insights into the bonding width achieved at each laser power. The 400 W joints exhibit the narrowest bonding width in the study (Fig. 10a), which explains their moderate lap-shear test performance (Fig. 9). Increasing laser power to 450 W and 500 W widens the melting width of CF/PEEK, resulting in high-quality joints with visible melted PEEK matrix on the Ti surface (Fig. 10b, Fig. 10c). A further increase in power leads to thermal damage in the CF/PEEK plates, impacting the joints mechanical performance (Fig. 9). As a matter of fact, formed porosities resulting from thermal degradation can be clearly seen in the fractured surfaces of the joints produced with laser powers ≥ 600 W (details of Fig. 10d - Fig. *10* Fig. 10f). Additionally, the applied thermal load at 700 W and 800 W has penetrated the top layers of CF/PEEK, rendering these powers unsuitable for the examined case study (Fig. 10e, Fig. 10f).

These observations are corroborated with SEM. Fig. 11 reveals that the 400 W and 450 W specimens exhibit primarily melting, with the latter approaching the thermal limits of CF/PEEK, as also shown by the model (Fig. 3, Table 2). At 500 W, thermal degradation initiates, evidenced by the exposed CFs in the centre of the applied laser beam (Fig. 11c). Laser powers > 500 W result in severe thermal damage,

with increased exposed fibers at 600 W (Fig. 11d) and penetration of the CF/PEEK plate at 700 W and 800 W (Fig. 11e, Fig. 11f). Finally, Fig. 11g - Fig. 11i show examples of porosities associated with the thermal degradation of CF/PEEK. These porosities act as delamination initiation points, leading to premature joint failure, impacting its performance (Fig. 9). Altogether, this analysis underscores the narrow process window of composite-metal laser joining applications. Despite the widening of the melting width with higher laser powers, the effective bonding width reduces upon thermal degradation. Therefore, achieving optimal composite-metal laser joining requires careful consideration of parameters that could attain high temperatures without inducing the polymer's thermal degradation mechanisms.

5.2.6. *Thermal degradation assessment: ATR-FTIR*

To assess the thermal damage in CF/PEEK, the fractured CF/PEEK plates are examined with ATR-FTIR. Five measurements are conducted on each specimen using a Nicolet iS50 FTIR spectrometer with a built-in diamond ATR from Thermo Fischer Scientific Inc. Spectra are collected from 4000 to 600 cm^{-1} with a resolution of 4 cm^{-1} and 128 scans, baseline-corrected, and normalised to the 1593 cm^{-1} peak [23,26,38,66]. Fig. 12a shows the spectral changes that occur in the CF/PEEK plates joined with laser powers up to 600 W. In the 700 W and 800 W specimens, the thermal damage is significant along the laser pathway (Fig. 10) and the accumulated spectra only capture the CF presence without identifiable PEEK peaks. This indicates complete PEEK degradation which agrees with the numerical model (Fig. 3, Table 2) and SEM results (Fig. 11). To a lesser extent, this is also the case for the 600 W specimen along the central line of its laser pathway. Nevertheless, to show the effect of an increased laser power on CF/PEEK, spectra from the HAZ boundaries at 600 W are presented in Fig. 12a together with the spectra of the 400 W, 450 W, and 500 W joints that exhibit a more consistent response. Altogether, spectral changes mostly occur in the 1800 – 600 cm^{-1} region and are attributed to the crosslinking that takes place in PEEK upon the event of thermal degradation [23,26,38,66]. In detail, a new fluorenone peak is formed at 1711 cm^{-1} and at 1452 cm^{-1}, a shoulder is found at the proximal ether peak at 1216 cm^{-1}, and changes at the diphenylether bonds are identified in the region around 1110 cm^{-1}. Finally, modifications in the aromatic hydrogens are detected at 863 cm^{-1} and 841 cm^{-1} [23,26,38,66].

To assess the extent of thermal degradation, the analysis focusses on the intensity of the 1711 cm^{-1} peak. This methodology has been outlined in a recent study by the authors where fluorenone's intensity was

associated with the resulting extent of thermal degradation after exposing PEEK and CF/PEEK in rapid high-temperature processing [26]. Fig. 12a shows that the 1711 cm^{-1} peak first forms at 450 W. Its intensity increases at higher laser powers which indicates the more significant thermal damage that is induced. To quantify this thermal damage, Fig. 12b presents the average peak intensity and standard deviation in the 450 W and 500 W specimens that had a more uniform spectral response. Additionally, fluorenone's intensity when PEEK is thermally degraded up to a mass loss of 0.5%, 1.2%, and 4% is also shown [26]. The results show that the PEEK matrix has experienced a thermal degradation slightly above 0.5%, and 1.2% after joining with 450 W and 500 W respectively. These values are close to those captured with the model and especially in the 500 W joints, a very good agreement is reached. Interestingly, the fact that 500 W - where the thermal damage slightly exceeds 1% - emerges as the critical laser power that first impacts the performance of the joints (Fig. 9) is noteworthy. It shows that a 1% degradation is the critical thermal threshold for PEEK in rapid heating conditions [26,58,62,63].

6. A short comparison between the experimental and numerical investigation

This study utilised the coupled thermal-chemical numerical model developed in [38] to simulate the laser joining of CF/PEEK with Titanium. The model accounts for the effect of the applied heating rate on the degradation mechanisms of the polymer matrix, and it was used to identify the laser joining parameters that slightly trigger the degradation mechanisms of CF/PEEK. To validate the model, ATR-FTIR was used, and an SEM analysis of the joints' cross sections and fractured CF/PEEK surfaces took place. A good agreement was found between the two investigations, and the main points can be summarized as follows. First, the model indicates that laser powers ≥ 600 W cause thermal defects on the Ti surface, in line with the experimental observations of Fig. 5. The model captures 500 W as the critical laser power initiating thermal damage in CF/PEEK, similar to SEM that first detects thermal degradation porosities at 500 W (Fig. 6c). At 700 W and 800 W, the model predicts complete degradation of PEEK, which is captured with SEM (Fig. 11), and with ATR-FTIR that indicates CF dominance at these powers. A similar, but less severe, response is also noted at 600 W (Fig. 11d, Fig. 12a). Finally, the intensity of the 1711 cm^{-1} peak aligns with the model's predictions of 1.22% degradation at 500 W, while a fair approximation is reached in the 450 W joints (Fig. 3b, Table 2, Fig. 12b). A recommended practice for further enhancing the model's accuracy would be to experimentally capture the exact beam profile, rather than relying solely on theoretical expressions of the Gaussian laser

beam (Eq. 5). Implementing this approach would lead to a more precise temperature distribution on the applied laser pathway, potentially aligning better with the response observed with SEM (Fig. 11).

7. Conclusions

The proposed methodology's applicability extends beyond composite-metal laser joining and it could be a useful tool for a range of applications where high-temperature - short-duration processing is used and thermal degradation is a potential issue. Even with precise temperature data, determining the onset of thermal damage in these fast heating conditions remains challenging, hinging on both reached temperatures and dwell time. The significance of this - especially in scenarios where the exact temperature-time combination is elusive - underscores the necessity for reliable experimental and numerical tools for detecting and preventing the event of thermal degradation when fast heating is applied. This work has made substantial contribution in this direction by showcasing how the developed numerical tool can mitigate the thermal damage in a fast-heating application of CF/PEEK by identifying the critical parameters that would prevent it. This advancement can enhance the reliability of thermoplastic composites, thereby advancing their industrial use in a range of applications currently dominated by thermosetting composites.

Acknowledgement

This publication was made possible by the sponsorship and support of TWI. The work was enabled through, and undertaken at, the National Structural Integrity Research Centre (NSIRC), a postgraduate engineering facility for industry-led research into structural integrity established and managed by TWI through a network of both national and international Universities.

References

[1] Pramanik A, Basak AK, Dong Y, Sarker PK, Uddin MS, Littlefair G, et al. Joining of carbon fibre reinforced polymer (CFRP) composites and aluminium alloys – A review. Compos Part A Appl Sci Manuf 2017;101:1–29. https://doi.org/https://doi.org/10.1016/j.compositesa.2017.06.007.

[2] Liu S, Zhou J, Li Y, Zhang X. Using reaction heat of laser-induced AlTiC interlayer to connect CFRTP/aluminum. Opt Laser Technol 2019;113:365–73. https://doi.org/https://doi.org/10.1016/j.optlastec.2018.12.044.

[3] Zaldivar RJ, Kim HI, Steckel GL, Patel D, Morgan BA, Nokes JP. Surface preparation for adhesive bonding of polycyanurate-based fiber-reinforced composites using atmospheric plasma treatment. J Appl Polym Sci 2011;120:921–31. https://doi.org/https://doi.org/10.1002/app.33261.

[4] Ahmed TJ, Stavrov D, Bersee HEN, Beukers A. Induction welding of thermoplastic

composites—an overview. Compos Part A Appl Sci Manuf 2006;37:1638–51. https://doi.org/https://doi.org/10.1016/j.compositesa.2005.10.009.

[5] Amancio-Filho ST, Bueno C, dos Santos JF, Huber N, Hage E. On the feasibility of friction spot joining in magnesium/fiber-reinforced polymer composite hybrid structures. Materials Science and Engineering: A 2011;528:3841–8. https://doi.org/https://doi.org/10.1016/j.msea.2011.01.085.

[6] Meng X, Huang Y, Xie Y, Li J, Guan M, Wan L, et al. Friction self-riveting welding between polymer matrix composites and metals. Compos Part A Appl Sci Manuf 2019;127:105624. https://doi.org/https://doi.org/10.1016/j.compositesa.2019.105624.

[7] Kumar R, Singh R, Ahuja IPS, Penna R, Feo L. Weldability of thermoplastic materials for friction stir welding- A state of art review and future applications. Compos B Eng 2018;137:1–15. https://doi.org/https://doi.org/10.1016/j.compositesb.2017.10.039.

[8] Nagatsuka K, Yoshida S, Tsuchiya A, Nakata K. Direct joining of carbon-fiber–reinforced plastic to an aluminum alloy using friction lap joining. Compos B Eng 2015;73:82–8. https://doi.org/https://doi.org/10.1016/j.compositesb.2014.12.029.

[9] Geng P, Ma H, Li W, Murakami K, Wang Q, Ma N, et al. Improving bonding strength of Al/CFRTP hybrid joint through modifying friction spot joining tools. Compos B Eng 2023;254:110588. https://doi.org/https://doi.org/10.1016/j.compositesb.2023.110588.

[10] Troschitz J, Vorderbrüggen J, Kupfer R, Gude M, Meschut G. Joining of Thermoplastic Composites with Metals Using Resistance Element Welding. Applied Sciences 2020;10. https://doi.org/10.3390/app10207251.

[11] Brassard D, Dubé M, Tavares JR. Resistance welding of thermoplastic composites with a nanocomposite heating element. Compos B Eng 2019;165:779–84. https://doi.org/https://doi.org/10.1016/j.compositesb.2019.02.038.

[12] Wippermann J, Meschut G, Koschukow W, Liebsch A, Gude M, Minch S, et al. Thermal influence of resistance spot welding on a nearby overmolded thermoplastic–metal joint. Welding in the World 2023;67:793 – 804. https://doi.org/10.1007/s40194-023-01465-y.

[13] Zhao T, Palardy G, Villegas IF, Rans C, Martinez M, Benedictus R. Mechanical behaviour of thermoplastic composites spot-welded and mechanically fastened joints: A preliminary comparison. Compos B Eng 2017;112:224–34. https://doi.org/https://doi.org/10.1016/j.compositesb.2016.12.028.

[14] Zhao G, Li M, Zhao Y, Zhou X, Yu H, Jian X, et al. Rotating gliding arc plasma: Innovative treatment for adhesion improvement between stainless steel heating elements and thermoplastics in resistance welding of composites. Compos B Eng 2024;272:111210. https://doi.org/https://doi.org/10.1016/j.compositesb.2024.111210.

[15] Rohart V, Laberge Lebel L, Dubé M. Improved adhesion between stainless steel heating element and PPS polymer in resistance welding of thermoplastic composites. Compos B Eng 2020;188:107876. https://doi.org/https://doi.org/10.1016/j.compositesb.2020.107876.

[16] Balle F, Emrich S, Wagner G, Eifler D, Brodyanski A, Kopnarski M. Improvement of Ultrasonically Welded Aluminum/Carbon Fiber Reinforced Polymer-Joints by Surface Technology and High Resolution Analysis. Adv Eng Mater 2013;15:814–20. https://doi.org/https://doi.org/10.1002/adem.201200282.

[17] Ma Z, Xu Z, Li Z, Chen S, Wu Y, Yan J. Improving the quality of resistance welded thermoplastic composite joints by applying ultrasonic. Compos B Eng 2024;277:111398. https://doi.org/https://doi.org/10.1016/j.compositesb.2024.111398.

[18] Tan X, Zhang J, Shan J, Yang S, Ren J. Characteristics and formation mechanism of porosities in CFRP during laser joining of CFRP and steel. Compos B Eng 2015;70:35–43. https://doi.org/https://doi.org/10.1016/j.compositesb.2014.10.023.

[19] Lambiase F, Genna S. Laser-assisted direct joining of AISI304 stainless steel with polycarbonate sheets: Thermal analysis, mechanical characterization, and bonds morphology. Opt Laser Technol 2017;88:205–14. https://doi.org/https://doi.org/10.1016/j.optlastec.2016.09.028.

[20] Jiao J, Zou Q, Ye Y, Xu Z, Sheng L. Carbon fiber reinforced thermoplastic composites and TC4 alloy laser assisted joining with the metal surface laser plastic-covered method. Compos B Eng 2021;213:108738. https://doi.org/https://doi.org/10.1016/j.compositesb.2021.108738.
[21] Bu H, Li X, Li B, Li X, Zhan X. Enhanced interfacial joining strength of laser wobble joined 6061-T6 Al alloy/CFRTP joint via interfacial bionic textures pre-construction. Compos B Eng 2023;261:110787. https://doi.org/https://doi.org/10.1016/j.compositesb.2023.110787.
[22] Su J, Wang X, Tan C, Sing SL, Liang S, Zhang X, et al. Directionally induced high-density secondary interaction for enhancing the bonding reliability of titanium alloy and CFRTP via functional Schiff base-contained polymer. Compos B Eng 2024;275:111316. https://doi.org/https://doi.org/10.1016/j.compositesb.2024.111316.
[23] Gaitanelis D, Chanteli A, Worrall C, Weaver PM, Kazilas M. A multi-technique and multi-scale analysis of the thermal degradation of PEEK in laser heating. Polym Degrad Stab 2023;211:110282. https://doi.org/https://doi.org/10.1016/j.polymdegradstab.2023.110282.
[24] Fernandez Villegas I, Vizcaino Rubio P. On avoiding thermal degradation during welding of high-performance thermoplastic composites to thermoset composites. Compos Part A Appl Sci Manuf 2015;77:172–80. https://doi.org/https://doi.org/10.1016/j.compositesa.2015.07.002.
[25] Stokes-Griffin CM, Compston P. An inverse model for optimisation of laser heat flux distributions in an automated laser tape placement process for carbon-fibre/PEEK. Compos Part A Appl Sci Manuf 2016;88:190–7. https://doi.org/https://doi.org/10.1016/j.compositesa.2016.05.034.
[26] Gaitanelis D, Worrall C, Kazilas M. Detecting, characterising and assessing PEEK's and CF-PEEK's thermal degradation in rapid high-temperature processing. Polym Degrad Stab 2022;204:110096. https://doi.org/https://doi.org/10.1016/j.polymdegradstab.2022.110096.
[27] Schricker K, Diller S, Bergmann JP. Bubble formation in thermal joining of plastics with metals. Procedia CIRP 2018;74:518–23. https://doi.org/https://doi.org/10.1016/j.procir.2018.08.132.
[28] Arkhurst BM, Seol JB, Lee YS, Lee M, Kim JH. Interfacial structure and bonding mechanism of AZ31/carbon-fiber-reinforced plastic composites fabricated by thermal laser joining. Compos B Eng 2019;167:71–82. https://doi.org/https://doi.org/10.1016/j.compositesb.2018.12.002.
[29] Jung K-W, Kawahito Y, Takahashi M, Katayama S. Laser direct joining of carbon fiber reinforced plastic to aluminum alloy. J Laser Appl 2013;25:032003. https://doi.org/10.2351/1.4794297.
[30] Katayama S, Kawahito Y. Laser direct joining of metal and plastic. Scr Mater 2008;59:1247–50. https://doi.org/https://doi.org/10.1016/j.scriptamat.2008.08.026.
[31] Wahba M, Kawahito Y, Katayama S. Laser direct joining of AZ91D thixomolded Mg alloy and amorphous polyethylene terephthalate. J Mater Process Technol 2011;211:1166–74. https://doi.org/https://doi.org/10.1016/j.jmatprotec.2011.01.021.
[32] Xia H, Ma Y, Chen C, Su J, Zhang C, Tan C, et al. Influence of laser welding power on steel/CFRP lap joint fracture behaviors. Compos Struct 2022;285:115247. https://doi.org/https://doi.org/10.1016/j.compstruct.2022.115247.
[33] Chen YJ, Yue TM, Guo ZN. A new laser joining technology for direct-bonding of metals and plastics. Mater Des 2016;110:775–81. https://doi.org/https://doi.org/10.1016/j.matdes.2016.08.018.
[34] Lionetto F, Mele C, Leo P, D'Ostuni S, Balle F, Maffezzoli A. Ultrasonic spot welding of carbon fiber reinforced epoxy composites to aluminum: mechanical and electrochemical characterization. Compos B Eng 2018;144:134–42. https://doi.org/https://doi.org/10.1016/j.compositesb.2018.02.026.
[35] Tan C, Su J, Liu Y, Feng Z, Song X, Wang X, et al. Enhanced interfacial bonding strength

of laser bonded titanium alloy/CFRTP joint via hydrogen bonds interaction. Compos B Eng 2022;239:109966. https://doi.org/https://doi.org/10.1016/j.compositesb.2022.109966.
[36] Bonmatin M, Chabert F, Bernhart G, Cutard T, Djilali T. Ultrasonic welding of CF/PEEK composites: Influence of welding parameters on interfacial temperature profiles and mechanical properties. Compos Part A Appl Sci Manuf 2022;162:107074. https://doi.org/https://doi.org/10.1016/j.compositesa.2022.107074.
[37] Lambiase F, Genna S, Kant R. A procedure for calibration and validation of FE modelling of laser-assisted metal to polymer direct joining. Opt Laser Technol 2018;98:363–72. https://doi.org/https://doi.org/10.1016/j.optlastec.2017.08.016.
[38] Gaitanelis D, Worrall C, Kazilas M. A numerical model to prevent the thermal degradation of CFRPs at extreme heating rates – The laser processing of CF/PEEK. Compos Part A Appl Sci Manuf 2024;177:107938. https://doi.org/https://doi.org/10.1016/j.compositesa.2023.107938.
[39] Lambiase F, Genna S. Homogenization of temperature distribution at metal-polymer interface during Laser Direct Joining. Opt Laser Technol 2020;128:106226. https://doi.org/https://doi.org/10.1016/j.optlastec.2020.106226.
[40] Mahmood T, Mian A, Amin MR, Auner G, Witte R, Herfurth H, et al. Finite element modeling of transmission laser microjoining process. J Mater Process Technol 2007;186:37–44. https://doi.org/https://doi.org/10.1016/j.jmatprotec.2006.11.225.
[41] Dhorajiya AP, Mayeed MS, Auner GW, Baird RJ, Newaz GM, Patwa R, et al. Finite Element Thermal/Mechanical Analysis of Transmission Laser Microjoining of Titanium and Polyimide. J Eng Mater Technol 2009;132. https://doi.org/10.1115/1.3184031.
[42] Rodríguez-Vidal E, Lambarri J, Soriano C, Sanz C, Verhaeghe G. A Combined Experimental and Numerical Approach to the Laser Joining of Hybrid Polymer – Metal Parts. Phys Procedia 2014;56:835–44. https://doi.org/https://doi.org/10.1016/j.phpro.2014.08.101.
[43] Jiao J, Ye Y, Jia S, Xu Z, Ouyang W, Zhang W. CFRTP -Al alloy laser assisted joining with a high speed rotational welding technology. Opt Laser Technol 2020;127:106187. https://doi.org/https://doi.org/10.1016/j.optlastec.2020.106187.
[44] Hussein FI, Salloomi KN, Akman E, Hajim KI, Demir A. Finite element thermal analysis for PMMA/st.st.304 laser direct joining. Opt Laser Technol 2017;87:64–71. https://doi.org/https://doi.org/10.1016/j.optlastec.2016.07.017.
[45] Jiao J, Wang Q, Wang F, Zan S, Zhang W. Numerical and experimental investigation on joining CFRTP and stainless steel using fiber lasers. J Mater Process Technol 2017;240:362–9. https://doi.org/https://doi.org/10.1016/j.jmatprotec.2016.10.013.
[46] O'Shaughnessey PG, Dubé M, Villegas IF. Modeling and experimental investigation of induction welding of thermoplastic composites and comparison with other welding processes. J Compos Mater 2016;50:2895–910. https://doi.org/10.1177/0021998315614991.
[47] Su J, Tan C, Wu Z, Wu L, Gong X, Chen B, et al. Influence of defocus distance on laser joining of CFRP to titanium alloy. Opt Laser Technol 2020;124:106006. https://doi.org/https://doi.org/10.1016/j.optlastec.2019.106006.
[48] Tan C, Su J, Zhu B, Li X, Wu L, Chen B, et al. Effect of scanning speed on laser joining of carbon fiber reinforced PEEK to titanium alloy. Opt Laser Technol 2020;129:106273. https://doi.org/https://doi.org/10.1016/j.optlastec.2020.106273.
[49] Martín MI, Rodríguez-Lence F, Güemes A, Fernández-López A, Pérez-Maqueda LA, Perejón A. On the determination of thermal degradation effects and detection techniques for thermoplastic composites obtained by automatic lamination. Compos Part A Appl Sci Manuf 2018;111:23–32. https://doi.org/https://doi.org/10.1016/j.compositesa.2018.05.006.
[50] Day M, Cooney JD, Wiles DM. The kinetics of the oxidattve degradation of poly(aryl-ether-ether-ketone) (PEEK). Thermochim Acta 1989;147:189–97. https://doi.org/https://doi.org/10.1016/0040-6031(89)85174-3.
[51] Patel P, Hull TR, McCabe RW, Flath D, Grasmeder J, Percy M. Mechanism of thermal

decomposition of poly(ether ether ketone) (PEEK) from a review of decomposition studies. Polym Degrad Stab 2010;95:709–18. https://doi.org/https://doi.org/10.1016/j.polymdegradstab.2010.01.024.

[52] Yao F, Zheng J, Qi M, Wang W, Qi Z. The thermal decomposition kinetics of poly(ether-ether-ketone) (PEEK) and its carbon fiber composite. Thermochim Acta 1991;183:91–7. https://doi.org/https://doi.org/10.1016/0040-6031(91)80448-R.

[53] Henderson JB, Tant MR, Moore GR, Wiebelt JA. Determination of kinetic parameters for the thermal decomposition of phenolic ablative materials by a multiple heating rate method. Thermochim Acta 1981;44:253–64. https://doi.org/https://doi.org/10.1016/0040-6031(81)85019-8.

[54] Hedberg GK, Shin YC. Laser Assisted Milling of Ti-6Al-4V ELI with the Analysis of Surface Integrity and its Economics. Lasers in Manufacturing and Materials Processing 2015;2:164–85. https://doi.org/10.1007/s40516-015-0013-4.

[55] Lisiecki A. Study of Optical Properties of Surface Layers Produced by Laser Surface Melting and Laser Surface Nitriding of Titanium Alloy. Materials 2019;12. https://doi.org/10.3390/ma12193112.

[56] Yang J, Sun S, Brandt M, Yan W. Experimental investigation and 3D finite element prediction of the heat affected zone during laser assisted machining of Ti6Al4V alloy. J Mater Process Technol 2010;210:2215–22. https://doi.org/https://doi.org/10.1016/j.jmatprotec.2010.08.007.

[57] Cogswell FN, editor. Subject Index. Thermoplastic Aromatic Polymer Composites, Butterworth-Heinemann; 1992, p. 263–8. https://doi.org/https://doi.org/10.1016/B978-0-7506-1086-5.50037-9.

[58] Sonmez FO, Hahn HT. Modeling of Heat Transfer and Crystallization in Thermoplastic Composite Tape Placement Process. Journal of Thermoplastic Composite Materials 1997;10:198–240. https://doi.org/10.1177/089270579701000301.

[59] Patel P, Hull TR, Lyon RE, Stoliarov SI, Walters RN, Crowley S, et al. Investigation of the thermal decomposition and flammability of PEEK and its carbon and glass-fibre composites. Polym Degrad Stab 2011;96:12–22. https://doi.org/https://doi.org/10.1016/j.polymdegradstab.2010.11.009.

[60] Courvoisier E, Bicaba Y, Colin X. Multi-scale and multi-technique analysis of the thermal degradation of poly(ether ether ketone). Polym Degrad Stab 2018;151:65–79. https://doi.org/https://doi.org/10.1016/j.polymdegradstab.2018.03.001.

[61] Day M, Cooney JD, Wiles DM. A kinetic study of the thermal decomposition of poly(aryl-ether-ether-ketone) (PEEK) in nitrogen. Polym Eng Sci 1989;29:19–22. https://doi.org/https://doi.org/10.1002/pen.760290105.

[62] Dolo G, Férec J, Cartié D, Grohens Y, Ausias G. Model for thermal degradation of carbon fiber filled poly(ether ether ketone). Polym Degrad Stab 2017;143:20–5. https://doi.org/https://doi.org/10.1016/j.polymdegradstab.2017.06.006.

[63] Colak ZS, Sonmez FO, Kalenderoglu V. Process Modeling and Optimization of Resistance Welding for Thermoplastic Composites. J Compos Mater 2002;36:721–44. https://doi.org/10.1177/0021998302036006507.

[64] Gaitanelis DG, Giannopoulos IK, Theotokoglou EE. Numerical FEA parametric analysis of CAI behaviour of CFRP stiffened panels. Thin-Walled Structures 2019;143. https://doi.org/10.1016/j.tws.2019.106231.

[65] Gaitanelis D, Williams CJ, Donoghue J, Frias C. A simplified methodology for assessing the interface of CFRPs with fibre push-out testing. Compos Part A Appl Sci Manuf 2025;190:108542. https://doi.org/https://doi.org/10.1016/j.compositesa.2024.108542.

[66] Gaitanelis D, Worrall C, Kazilas M. Influence of rapid high-temperature processing on the interface of CF/PEEK: A quick and effective method for enhancing the IFSS. Compos Sci Technol 2024:110564. https://doi.org/https://doi.org/10.1016/j.compscitech.2024.110564.

[67] Griffis CA, Nemes JA, Stonesifer FR, Chang CI. Degradation in Strength of Laminated

Composites Subjected to Intense Heating and Mechanical Loading. J Compos Mater 1986;20:216–35. https://doi.org/10.1177/002199838602000301.

[68] Rawal SP, Misra MS. Measurement of Mechanical and Thermophysical Properties of Dimensionally Stable Materials for Space Applications. NASA Contractor Report 1992;189552.

[69] Cogswell FN, editor. Subject Index. Thermoplastic Aromatic Polymer Composites, Butterworth-Heinemann; 1992, p. 263–8. https://doi.org/10.1016/B978-0-7506-1086-5.50037-9.

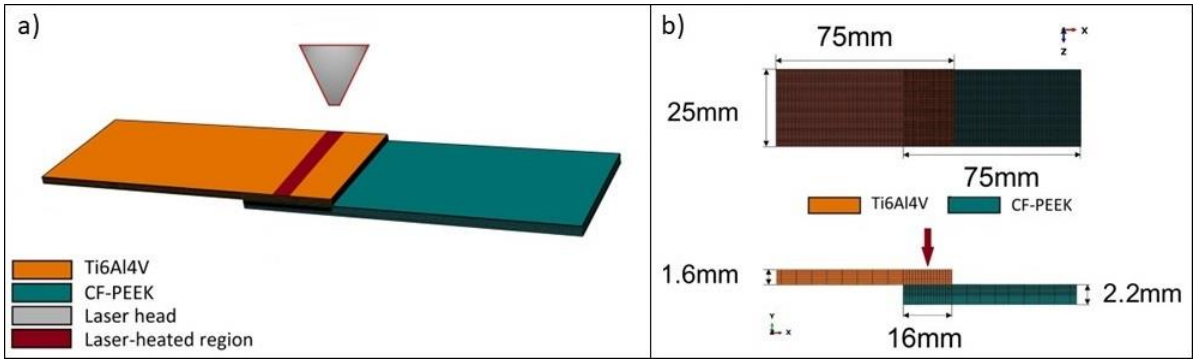

Fig. 1. a) Schematic figure of the laser joining process and b) Dimensions and mesh regions of the examined lap-joint configuration.

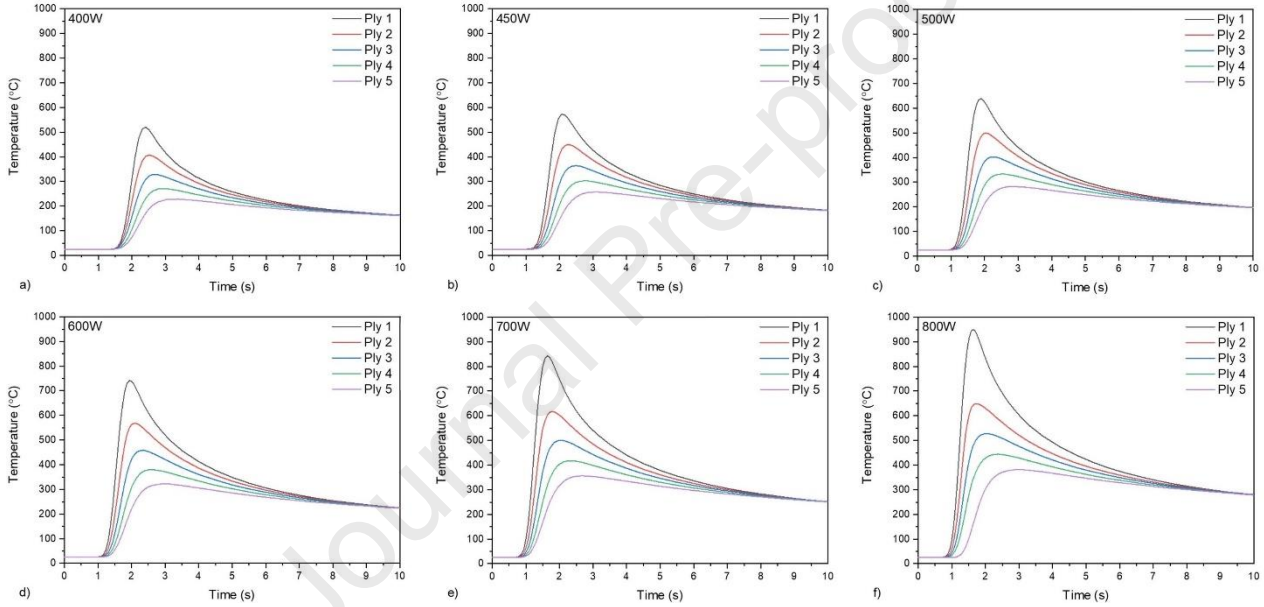

Fig. 2. Through-thickness temperature profiles of the top five plies of CF/PEEK after laser joining with the Ti alloy at the examined laser powers: a) 400 W, b) 450 W, c) 500 W, d) 600 W, e) 700 W, and f) 800 W.

.

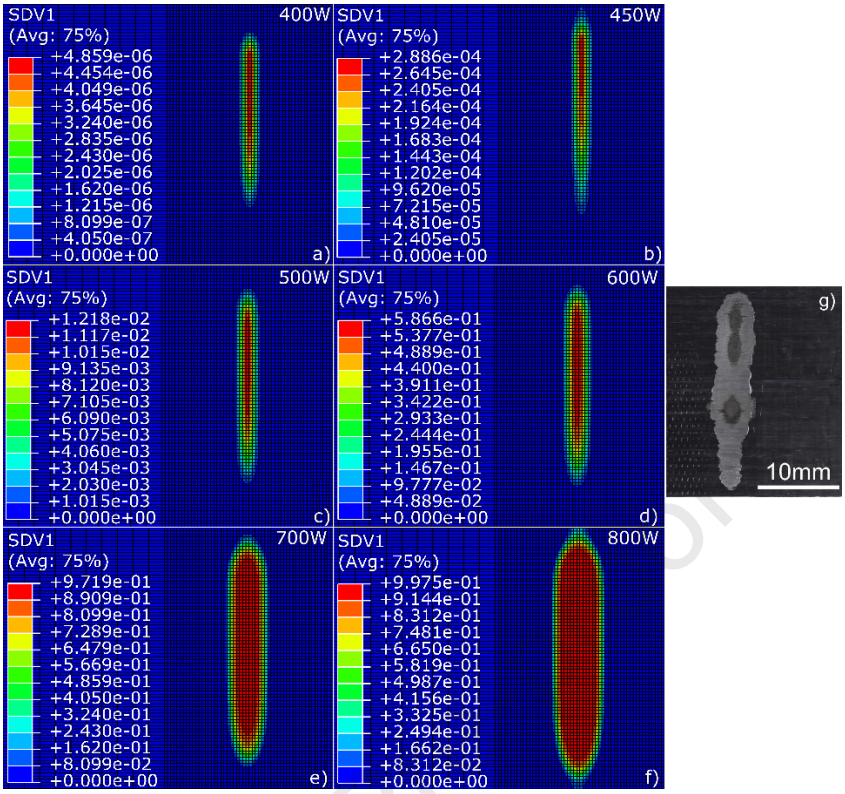

Fig. 3. a) – f) Decomposition degree field on the surface of CF/PEEK after laser joining with the Ti alloy at the examined laser powers, and g) Representative Heat-Affected Zone (HAZ) observed after the laser joining trials.

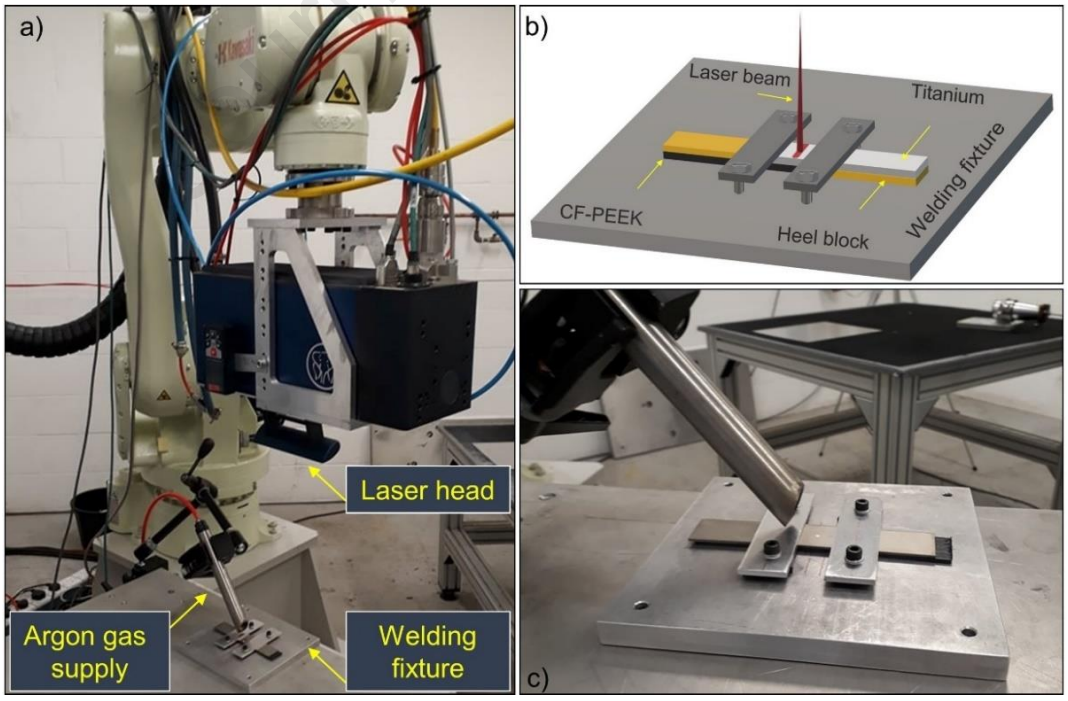

Fig. 4. Experimental setup: a) IPG YLS-2000 fiber laser with a maximum power of 2 kW and a wavelength of 1070 nm, argon gas supplier, and welding fixture, b) joining process schematic, and c) clamping system.

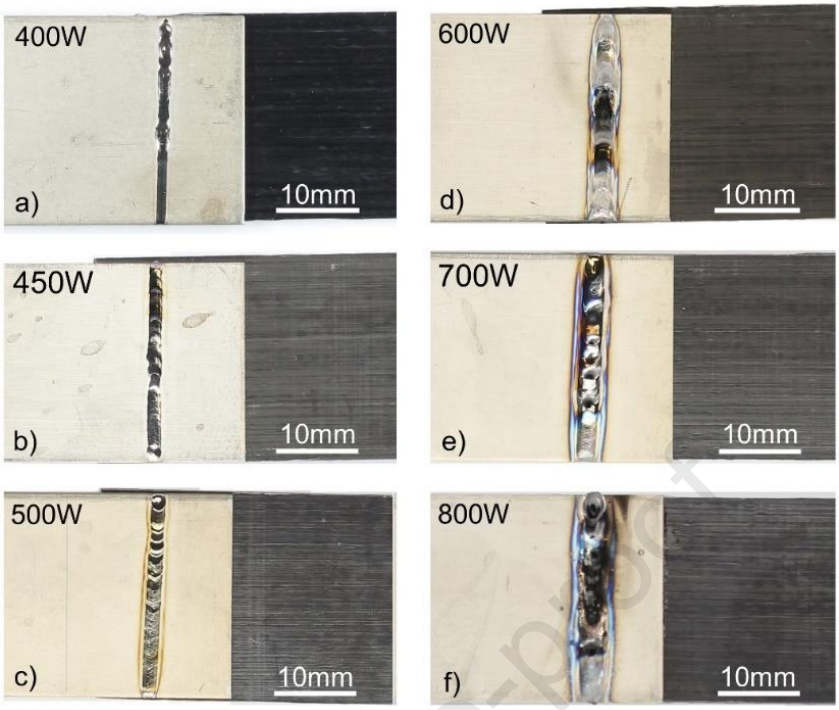

Fig. 5. Surface of the CF/PEEK-Ti joints after laser joining with the examined laser powers.

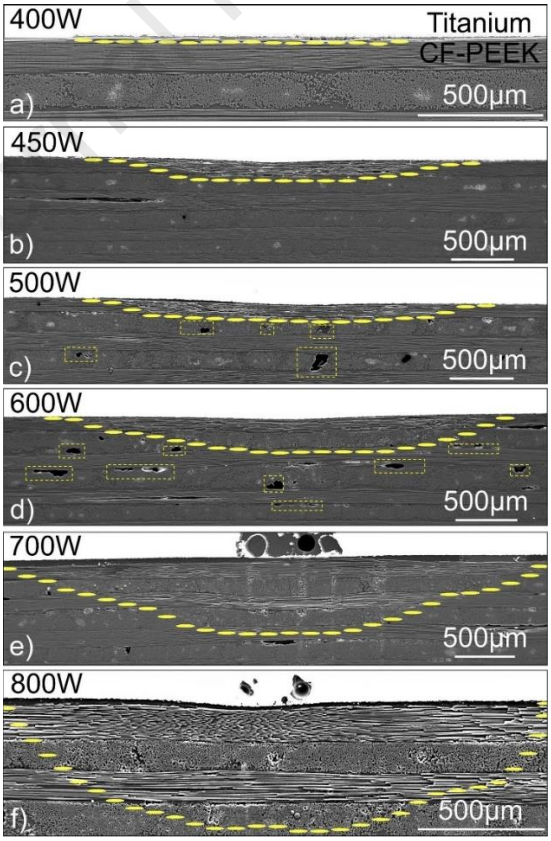

Fig. 6. Cross-sections of the CF/PEEK-Ti joints after laser joining with the examined laser powers.

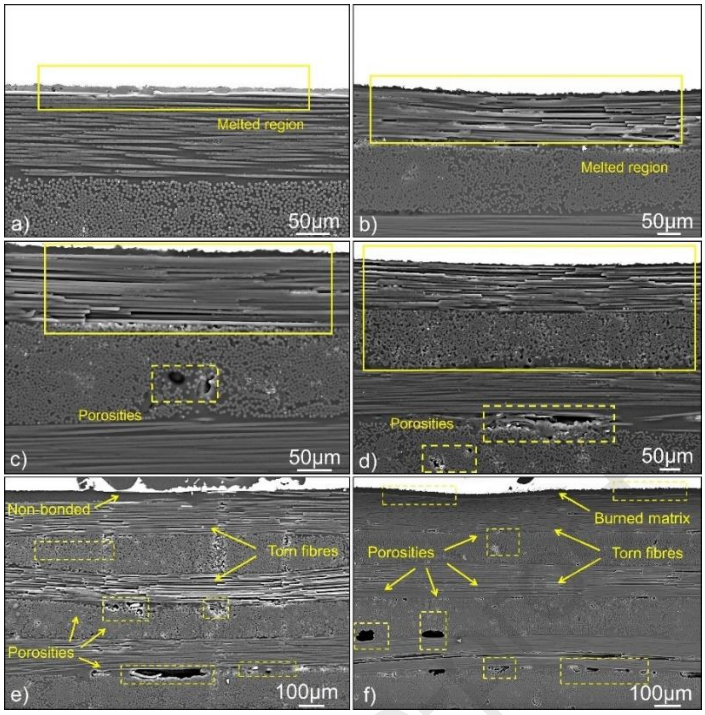

Fig. 7. Cross-sectional microstructure of the CF/PEEK-Ti joints produced with: a) 400 W, b) 450 W, c) 500 W, d) 600 W, e) 700 W, and f) 800 W.

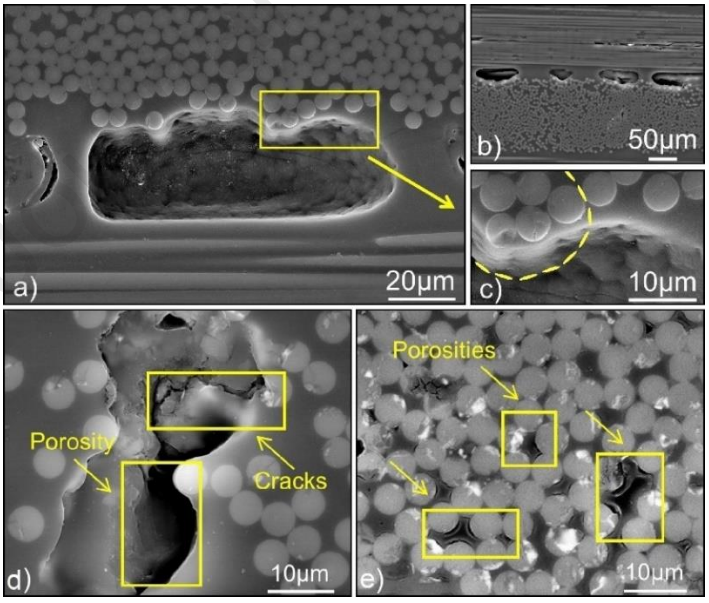

Fig. 8. Observed types of porosities: a) Thermal degradation porosities at a) 500 W, and b) 600 W. Shrinkage porosities d) due to CF/PEEK's solidification sequence at 500 W, and e) due to thermal residual stresses between CFs and PEEK at 800 W. c) Thermal residual stresses around the 500 W porosity.

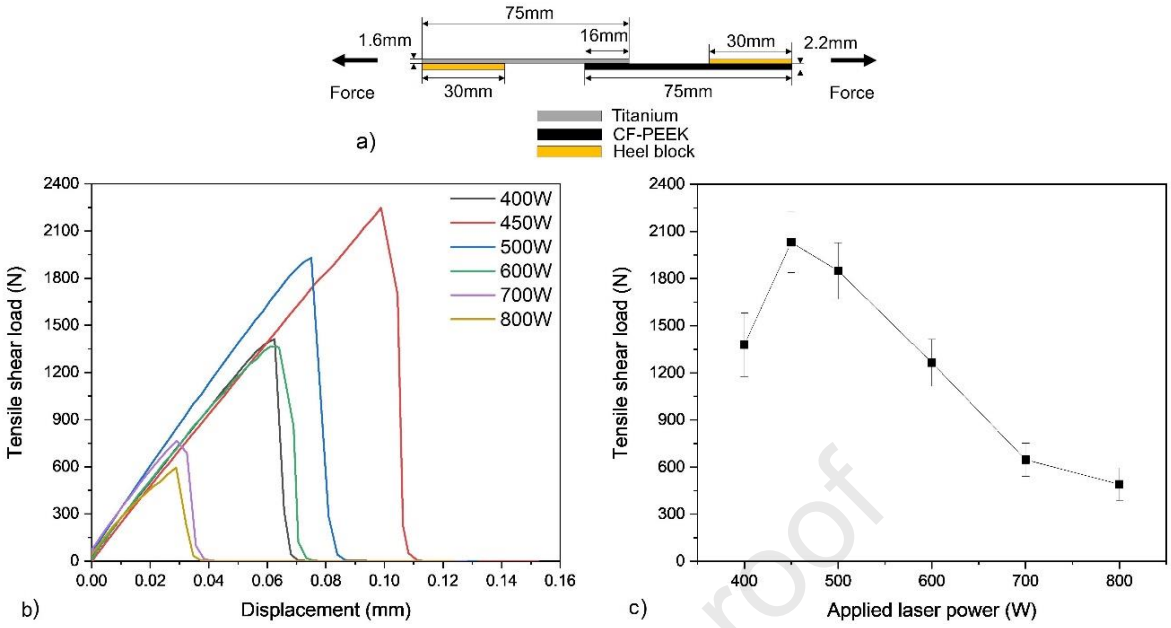

Fig. 9. a) Schematic figure of the performed lap-shear tests, b) representative tensile shear load - displacement curves, and b) average value and standard deviation of the tensile shear load of the CF/PEEK-Ti joints produced with the examined lasers powers.

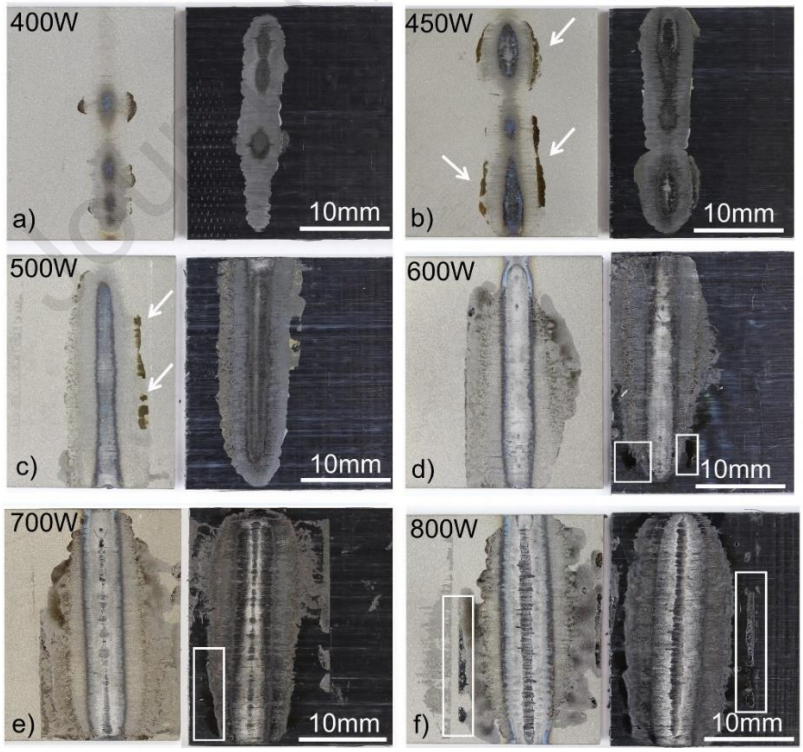

Fig. 10. Fractured surfaces of the examined CF/PEEK-Ti joints after the examined laser joining.

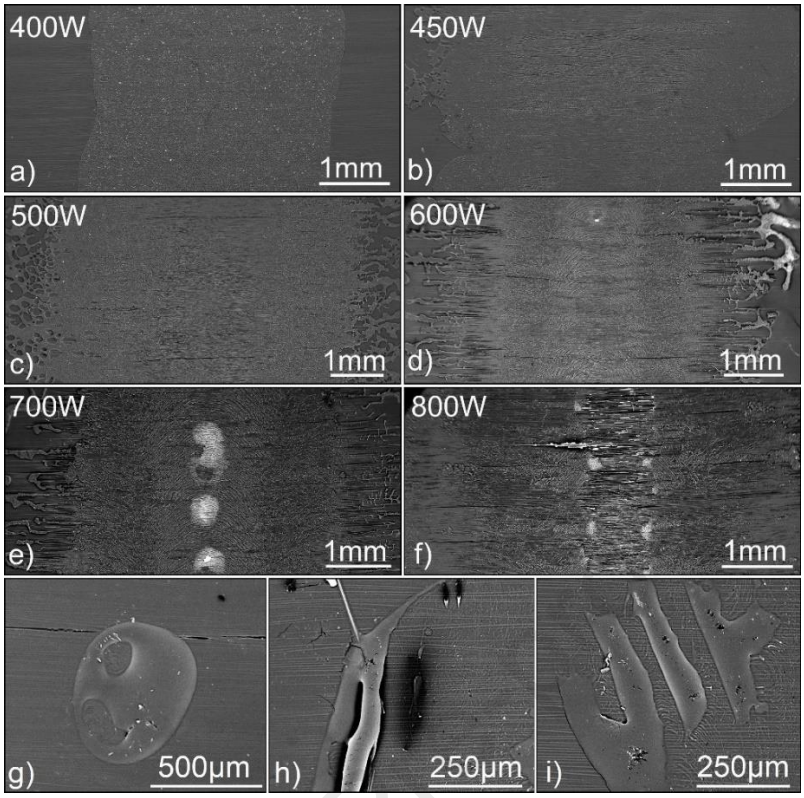

Fig. 11. a) – f) Fractured surfaces of CF/PEEK after laser joining with the examined lasers powers and formed porosities at the fractured CF/PEEK surface of the joints produced with g) 600 W and h), i) 700 W.

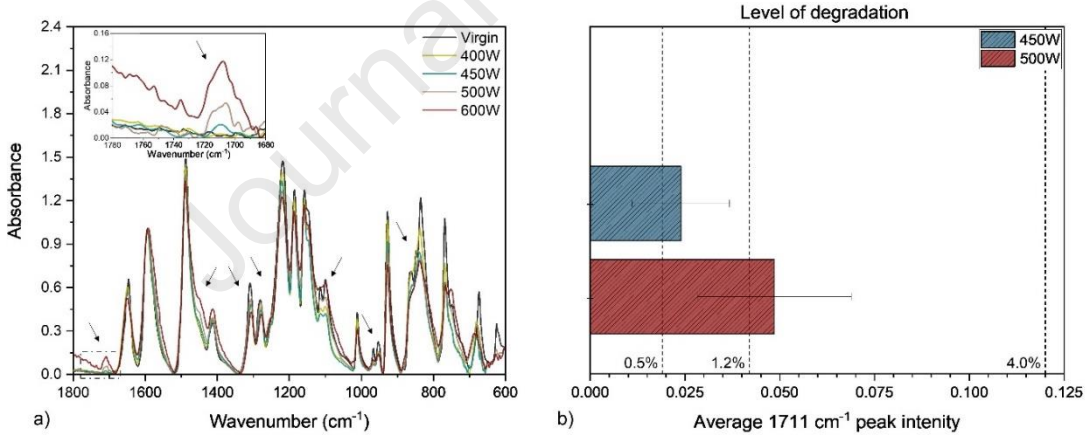

Fig. 12. a) Spectral changes in CF/PEEK after laser joining with powers up to 600 W, and detail of the 1711 cm^{-1} peak intensity at these powers. b) Resulting extent of degradation at the fractured CF/PEEK surfaces of the joints produced with 450 W and 500 W, as captured by the 1711 cm^{-1} peak intensity.

Table 1. Decomposition-dependent material properties of CF/PEEK [67–69] and kinetic parameters of PEEK implemented in the model [38].

Decomposition degree α	Thermal conductivity (W/m·K)			Specific heat (J/kg·K)	Density (kg/m^3)
	Longitudinal	Transverse	Through-thickness		
0	4.1	0.47	0.47	823	1590
1	1.736	0.1	0.1	2171	1270.4
Activation energy E_a (kJ/mol): 182.09, Pre-exponential factor A (1/sec): 4.27 × 1013, Reaction order n: 2.2					

Table 2. Main outputs of the numerical investigation: Maximum reached temperatures at the surface of Titanium and CF/PEEK, and maximum reached decomposition degree α in the first ply of CF/PEEK.

Laser power (W)	Ti surface	CF/PEEK: First ply	
	Temperature (°C)	Temperature (°C)	Decomposition degree α
400	816	520	4.86×10^{-6}
450	884	574	2.89×10^{-4}
500	954	639	1.22×10^{-2}
600	1091	742	5.86×10^{-1}
700	1222	844	9.72×10^{-1}
800	1350	950	9.98×10^{-1}

Highlights

- A methodology is proposed for detecting the thermal limits of thermoplastic composites in thermal joining applications with metals.
- The model's applicability is demonstrated in a laser joining case study of CF/PEEK with Titanium.
- The experimental investigation shows that the model accurately detects the critical parameters that first trigger the thermal degradation of CF/PEEK.
- Those are the critical processing conditions that first deteriorate the performance of the joints.
- The proposed numerical framework can be used to optimise a range of joining applications where fast heating is involved and thermal degradation is a potential issue.

Declaration of interests

☒ The authors declare that they have no known competing financial interests or personal relationships that could have appeared to influence the work reported in this paper.

☐ The authors declare the following financial interests/personal relationships which may be considered as potential competing interests: